Noname manuscript No.
(will be inserted by the editor)

A quasistatic ALE cable formulation for multibody systems applications

Olivier Devigne · Alejandro Cosimo · Olivier Brüls

Received: 12 February 2024 / Accepted: 4 October 2024

Abstract This paper presents an arbitrary Lagrangian-Eulerian (ALE) formulation for a quasistatic cable finite element. The objective is to propose a theoretical framework for the derivation of the ALE equilibrium equations of the cable starting from a continuous formulation and the principle of virtual work. The model aims to be simple, as only axial strains are considered. The advantages of using an ALE formulation are also shown through several numerical examples. In the case of a distributed loading, the ALE setting yields an energy-optimal mesh. In some cases, the problem can be nonconvex and a regularization of the equations is proposed to ensure the convergence of the Newton solver to one of the solutions. A cable-pulley system is also investigated without and with friction. In the latter case, the results are validated with an analytical formula for the evolution of the tension force in the cable. Finally, a multibody model of a soft finger is proposed in which the coupling of a system of rigid bodies with the cable model is enforced through kinematic constraints.

Keywords Arbitrary Lagrangian-Eulerian formulation · multibody systems · cable · cable-pulley systems · finite element method

1 Introduction

Cables are part of many engineering applications, such as suspended bridges or power lines. For this reason, cable modeling has been investigated for more than a century. In these two examples, due to the sag and length of the cables, vibrations need to be considered. In this context, one of the first investigations on the dynamics of cable was made by Rohrs [39], who determined the resonance frequencies for an inextensible cable. More than a century later, Irvine and Caughey [21, 22] unified all the previous developments made on cables with experimental validation. Wu *et al.* [44] then extended Irvine's theory to account for the presence of hybrid vibration modes

Olivier Devigne
University of Liège, Liège, Belgium
E-mail: o.devigne@uliege.be

Alejandro Cosimo
University of Liège, Liège, Belgium

Olivier Brüls
University of Liège, Liège, Belgium

(modes that are neither symmetric nor antisymmetric). All these authors considered a linear response of the cable. Nonetheless, nonlinear formulations have also been proposed, notably with the work of Hagedorn and Schäfer [15], who coupled Ritz-Galerkin and perturbation methods. Rega can be cited for his work on the comparison between several cable models [36] and a cable-oriented review [37]. Lacarbonara and Pacitti [25], along with Arena *et al.* [1] then studied a collection of important modeling aspects of cables with a specific attention paid to the bending stiffness, the torsional stiffness, and the noncompressibility of the cable. Research on the topic is still going on to this day [3].

Nevertheless, cables are not only structures attached at both ends to withstand a traction force. They can move, slide and even make contact and interact with other components of a multibody system. It is namely the case in reeving systems, deployable space structures or even in soft robotics. In such contexts, particularly when the system is operating in steady-state or at slow speed, vibrations are no longer the main concern, and elastic bar or elastic beam models can be used in a quasistatic setting.

A popular way of dealing with slender structures in multibody systems is to follow a nonlinear finite element method (FEM). However, in applications where the cable enters contact with a mechanical component, for instance in reeving systems where the cable is in contact with pulleys, there is a need for a fine discretization of the cable to accurately describe the frictional contact interactions. Nevertheless, it should be noted that this fine discretization is only needed in some key regions, i.e., along the pulley in this case. Unfortunately, because the cable is moving along the pulley with time, it is often necessary to work with smaller elements than needed along the whole cable length. In order to circumvent this difficulty, a popular option is to use an arbitrary Lagrangian-Eulerian (ALE) formulation. ALE formulations are widely used in fluid mechanics, see for instance [7], for example in fluid-structure problems, where the flow can be analyzed using an Eulerian viewpoint, whereas the structure deformation is analyzed using a Lagrangian viewpoint [24]. In the cable-pulley system, this approach permits one to fix the mesh to nonmaterial points of the cable, e.g., along a pulley span, and to account for a flow of material through each element of the mesh. The aim of this paper is to develop a quasistatic ALE cable formulation for the numerical simulation of such multibody systems.

For mechanical systems, the ALE equations can be derived starting from a continuous formulation, either by writing the balance of mass and momentum on a nonmaterial control volume [20] or by using variational principles, as proposed in [34]. In such frameworks, the nodes of the finite element mesh can have Lagrangian and Eulerian motions simultaneously. In [2,23], an ALE formulation based on a continuous variational framework is proposed in which the integrals are written on a referential domain. The authors highlight the fact that both the numerical solution and the mesh configuration then achieve a minimum of the potential energy. In other words, an optimal mesh is obtained with respect to the applied loading. In [29,45], a similar formulation named the "r-adaptive finite element method" is presented. In this case, the method leads to an optimal mesh and is also applied in fracture mechanics where the mesh adaptation permits one to follows the crack propagation. Another early and fundamental contribution to ALE formulations in fracture mechanics can be found in [27]. The possible redundancy and singularities of the ALE equations are investigated in [2,29], and specific regularization procedures are proposed to tackle this problem.

Several authors particularize the continuous approach to 1D structures, such as beams [32,35]. In [40], several approaches to model sliding beams, i.e., beams that undergo a large translational motion with a superimposed flexible deformation, were compared. A formulation based on a variational principle was developed in [19] for the modeling of sliding beams in which the integrals are written on a referential domain. The large vibrations of axially moving beams or strings were treated using an ALE approach in [41]. A mathematical model for dry friction in a cable-

pulley system is proposed in [31] using an Eulerian description. In [13], an Eulerian description is adopted to investigate a complex belt-pulley system. In [16], an ALE formulation for sliding beams is developed with a special emphasis on the configurational forces arising from the material flow. In this case, the equations were obtained using Reynold's transport theorem. This model was then used for the modeling of flexible multibody systems in [17]. In all these papers on ALE methods for 1D structures, no mention is made about the need for a regularization procedure to fix redundancy and singularity issues.

Another approach to derive the ALE equations for multibody systems is to start from the discretized form of the equations of motion and distinguish nodes with a purely Lagrangian description and nodes with a purely Eulerian description, thereby requiring specific ALE element formulations. This distinction eliminates the redundancy and singularity problems and thus the need for a regularization, but restricts the simulation to systems where no mesh optimality is sought. In [18], an ALE-ANCF element is developed for the modeling of a sliding joint. In [8], another ALE-ANCF approach for a beam element is developed to model reeving systems. In [9], similar reeving systems are studied using ALE elements based on a modal description of the deformation. In [33], an ALE element is developed to represent the part of the cable in contact with the pulley. Deployable space structures such as antennas are investigated in [11] using an ALE approach to model the cable-pulley-actuated system. An ALE cable-like model is developed in [14] for the modeling of muscle-tendon units in musculoskeletal systems.

In this paper, we propose to adapt the framework developed in [23] to model cables as unidimensional elements with a uniform distribution of axial strains in the cross section. Another contribution is to enable the simulation of multibody systems by the introduction of constraints. The formulation starts from a continuous form in which the integrals are written on the referential domain, inducing a consistent description of the problem in terms of the quasistatic spatial and material equilibria. As in [2], optimal meshes can be obtained, which offers interesting perspectives in multibody applications. In this quasistatic formulation, the redundancy and singularity problems are inherent to the ALE equations. To counteract this problem, a regularization technique, different from the one proposed in [2] or in [29], is presented. The optimal-mesh behavior, the possibility to model multibody systems with constraints and the effectiveness of the regularization will be studied through diversified examples.

The rest of the paper is organized as follows. In Section 2, the general ALE framework is first proposed along with the definition of the different quantities and domains of interest. After introducing kinematic assumptions, the continuous ALE equilibrium equations are derived for the proposed cable element. In Section 3, the discretization of the equilibrium equations is performed and the constraint vector is introduced in order to generalize the formulation to multibody systems. Due to the redundant nature of the quasistatic formulation, a regularization of the problem is also proposed. In Section 4, numerical examples are exposed, such as a cable-pulley system, a cable-actuated soft finger and a simpler demonstrative example. In Section 5, a brief discussion is conducted. Finally, in Section 6, conclusions are drawn and perspectives are considered.

2 Continuous ALE formulation

2.1 General ALE concept in 3D

The motion of particles is usually observed based on either a Lagrangian description or an Eulerian description. For any three-dimensional structure, one can define the material domain, denoted $\mathcal{B}_0$, and the spatial domain, denoted $\mathcal{B}_t$. In a purely Lagrangian description, a mapping

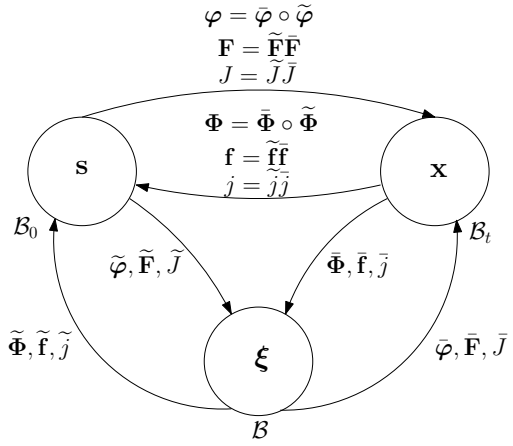

FIG. 1 – The referential domain enables us to decompose the total motion into a material and a spatial contribution. The three domains are interconnected by mappings, deformation gradients and Jacobians.

from the material domain to the spatial domain can be defined. This mapping tracks an arbitrary material particle on the structure with material coordinates $\mathbf{s} \in \mathbb{R}^3$ to its spatial location $\mathbf{x} \in \mathbb{R}^3$ and is written as $\mathbf{x} = \boldsymbol{\varphi}(\mathbf{s}, t)$. In a purely Eulerian description, the inverse mapping is involved, which tracks the flow of material through fixed spatial locations and can in turn be written as $\mathbf{s} = \boldsymbol{\Phi}(\mathbf{x}, t)$.

In an ALE approach, the motion is analyzed with both descriptions simultaneously, so that the total motion can be decomposed into a Lagrangian contribution and an Eulerian contribution. In order to make this decomposition, a third domain, called the referential domain and denoted $\mathcal{B}$, is defined. In general, the referential domain does not correspond to the material nor to the spatial domain. The equations of motion are expressed in this domain and represent the contributions of the Lagrangian part of the motion, which will be called the spatial motion, and the Eulerian part of the motion, which will be called the material motion. The purpose of this referential domain is thus to obtain two sets of equations to analyze the two distinct contributions to the motion separately.

The material motion is represented by a mapping from the referential domain to the material domain

$$\mathbf{s} = \widetilde{\boldsymbol{\Phi}}(\boldsymbol{\xi}, t) \tag{1}$$

The associated tangent map must be understood as a deformation gradient and is defined as $\widetilde{\mathbf{f}} \equiv \partial\widetilde{\boldsymbol{\Phi}}/\partial\boldsymbol{\xi}$, with the corresponding Jacobian $\widetilde{j} = \det\widetilde{\mathbf{f}}$. The inverse map from the material domain to the referential domain, the associated deformation gradient and Jacobian can be trivially expressed as $\widetilde{\boldsymbol{\varphi}} = \widetilde{\boldsymbol{\Phi}}^{-1}$, $\widetilde{\mathbf{F}} \equiv \partial\widetilde{\boldsymbol{\varphi}}/\partial\mathbf{s} = \widetilde{\mathbf{f}}^{-1}$ and $\widetilde{J} = \det\widetilde{\mathbf{F}} = \widetilde{j}^{-1}$. On the other hand, the mapping from the referential domain to the spatial domain, i.e., the spatial motion, is expressed as

$$\mathbf{x} = \bar{\boldsymbol{\varphi}}(\boldsymbol{\xi}, t) \tag{2}$$

The associated tangent map must also be understood as a deformation gradient and is defined as $\bar{\mathbf{F}} \equiv \partial\bar{\boldsymbol{\varphi}}/\partial\boldsymbol{\xi}$, with the corresponding Jacobian $\bar{J} \equiv \det\bar{\mathbf{F}}$. The inverse map from the spatial domain to the referential domain, the associated deformation gradient and Jacobian can again

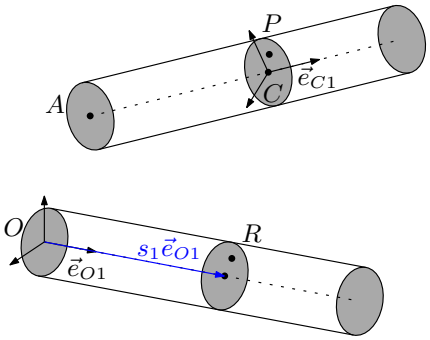

FIG. 2 – Cable model before and after deformation.

be trivially expressed as $\bar{\boldsymbol{\Phi}} = \bar{\boldsymbol{\varphi}}^{-1}$, $\bar{\mathbf{f}} \equiv \partial\bar{\boldsymbol{\Phi}}/\partial\mathbf{x} = \bar{\mathbf{F}}^{-1}$ and $\bar{j} = \det\bar{\mathbf{f}} = \bar{J}^{-1}$. Figure 1 graphically shows the connections between the different mappings, deformation gradients and Jacobians defined above. It can also be noted that the direct link between the material and the spatial domain is obtained through the composition of the mappings and tangent mappings previously defined:

$$\boldsymbol{\varphi} = \bar{\boldsymbol{\varphi}} \circ \widetilde{\boldsymbol{\Phi}}^{-1} = \boldsymbol{\Phi}^{-1} \tag{3}$$

$$\boldsymbol{\Phi} = \widetilde{\boldsymbol{\Phi}} \circ \bar{\boldsymbol{\varphi}}^{-1} = \boldsymbol{\varphi}^{-1} \tag{4}$$

$$\mathbf{F} = \bar{\mathbf{F}}\,\widetilde{\mathbf{F}} = \mathbf{f}^{-1} = \widetilde{\mathbf{f}}\,\bar{\mathbf{f}} \tag{5}$$

$$J = \bar{J}\,\widetilde{J} = j^{-1} = \widetilde{j}\,\bar{j} \tag{6}$$

In a continuous context, $\boldsymbol{\xi} \in \mathbb{R}^3$ can be understood as the set of points of interest of the structure. A more tangible meaning of this variable can be appreciated when thinking about a discretized formulation, which will be further investigated in Section 3: it describes the mesh. In that case, the spatial motion describes the motion of the mesh, whereas the material motion describes the flow of material through the mesh.

2.2 Cable kinematics

According to Fig. 2, in the reference undeformed configuration, the cable, of undeformed length L_0, is assumed to be aligned with the base vector $\vec{e}_{O1}$ and to have a uniform cross section. In this paper, the notation $\vec{\bullet}$ denotes a vector as a geometrical object and the bold notation represents its components expressed in a specific basis. For example, $\mathbf{e}_1 = \begin{bmatrix}1\ 0\ 0\end{bmatrix}^T$, $\mathbf{e}_2 = \begin{bmatrix}0\ 1\ 0\end{bmatrix}^T$ and $\mathbf{e}_3 = \begin{bmatrix}0\ 0\ 1\end{bmatrix}^T$ are the components of the geometric vectors $\vec{e}_{O1}$, $\vec{e}_{O2}$, $\vec{e}_{O3}$ in their own basis. The centerline is a straight line that starts at the origin O of the coordinate system, so that it is described by the set of particles with material coordinates $s_1\mathbf{e}_1$ for $s_1 \in \mathcal{L}_0 = [0, L_0]$. At a given point $s = s_1$ along the centerline, an arbitrary particle located at point R on the cross section is defined by its material position with respect to the frame $\{O, \vec{e}_{O1}, \vec{e}_{O2}, \vec{e}_{O3}\}$

$$\mathbf{x}_{OR} = \mathbf{s} = s\mathbf{e}_1 + s_2\mathbf{e}_2 + s_3\mathbf{e}_3 \tag{7}$$

which implies that the cross section is orthogonal to the centerline.

The motion from the reference to the deformed configuration is such that the cable can freely translate, rotate and deform. After motion, the cable has a length L_t, and the particle initially

in O has moved to point A. As can be seen in Fig. 2, the centerline particle is now located at point C with position $\mathbf{x}_{OC}$. Assuming that the cross section remains undeformed, the considered arbitrary particle on the cross section has moved from point R to point P with the spatial position

$$\mathbf{x} = \mathbf{x}_{OP}(s, s_2, s_3, t) = \mathbf{x}_{OC}(s, t) + \mathbf{R}_{OC}(s, t)\, \mathbf{x}_{CP}(s_2, s_3) \tag{8}$$

where $\mathbf{x}_{CP}(s_2, s_3) = s_2\mathbf{e}_2 + s_3\mathbf{e}_3$ is the position of P expressed in the cross-sectional frame $\{C, \vec{e}_{C1}, \vec{e}_{C2}, \vec{e}_{C3}\}$ and $\mathbf{R}_{OC}$ is the rotation matrix which represents the relative orientation between the frames $\{O, \vec{e}_{O1}, \vec{e}_{O2}, \vec{e}_{O3}\}$ and $\{C, \vec{e}_{C1}, \vec{e}_{C2}, \vec{e}_{C3}\}$. The above expression represents the mapping $\boldsymbol{\varphi}$ from the material to the spatial domain.

The Green-Lagrange strain tensor, $\mathbf{E}$, is defined using the deformation gradient $\mathbf{F}$ from the material to the spatial domain as

$$\mathbf{E} = \frac{1}{2}\left(\mathbf{F}^T\mathbf{F} - \mathbf{I}\right) \tag{9}$$

Using Eq. (8), $\mathbf{F}$ is expressed as

$$\mathbf{F} = \left[\frac{\partial \mathbf{x}}{\partial s}\ \frac{\partial \mathbf{x}}{\partial s_2}\ \frac{\partial \mathbf{x}}{\partial s_3}\right] = \left[\frac{\partial \mathbf{x}_{OC}}{\partial s} + \frac{\partial \mathbf{R}_{OC}}{\partial s}\,\mathbf{x}_{CP} \quad \mathbf{R}_{OC}\,\mathbf{e}_2 \quad \mathbf{R}_{OC}\,\mathbf{e}_3\right] \tag{10}$$

Let us introduce the curvilinear abscissa $x^\star \in [0, L_t]$. The axial gradient is then defined as $F = \partial x^\star/\partial s$. From the definition of the curvilinear abscissa, we have

$$F = \left\| \frac{\partial \mathbf{x}_{OC}}{\partial s} \right\| \tag{11}$$

and, exploiting the fact that $\mathbf{R}_{OC}\,\mathbf{e}_1$ is the unit vector in the direction of $\partial \mathbf{x}_{OC}/\partial s$,

$$\frac{\partial \mathbf{x}_{OC}}{\partial s} = F\,\mathbf{R}_{OC}\,\mathbf{e}_1 \tag{12}$$

In a cable model, the structure is considered slender, so that $\mathbf{x}_{CP}$ is small. The following kinematic approximation is thus considered for the evaluation of the strain energy:

$$\frac{\partial \mathbf{x}}{\partial s} = \frac{\partial \mathbf{x}_{OC}}{\partial s} + \frac{\partial \mathbf{R}_{OC}}{\partial s}\,\mathbf{x}_{CP} \approx \frac{\partial \mathbf{x}_{OC}}{\partial s} \tag{13}$$

which means that the deformation gradient is assumed to be purely axial and uniformly distributed in the cross section. From Eqs. (11) and (13), we obtain

$$F = \left\| \frac{\partial \mathbf{x}}{\partial s} \right\| \tag{14}$$

and from Eqs. (10) and (12)

$$\mathbf{F} = \mathbf{R}_{OC}\left[F\mathbf{e}_1\ \mathbf{e}_2\ \mathbf{e}_3\right] \tag{15}$$

The Green-Lagrange strain tensor is obtained as

$$\mathbf{E} = \begin{bmatrix} \frac{1}{2}\left(F^2 - 1\right) & 0 & 0 \\ 0 & 0 & 0 \\ 0 & 0 & 0 \end{bmatrix} \tag{16}$$

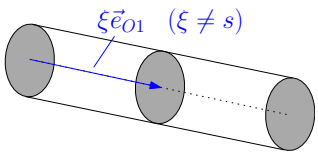

FIG. 3 – Referential domain for the cable.

It can be noted that only the axial strain $\varepsilon = \frac{1}{2}\left(F^2 - 1\right)$ is relevant to the problem. The Green-Lagrange strain tensor is thus only governed by the material coordinate s and the curvilinear coordinate $x^\star$.

In general, the referential domain is described by $\boldsymbol{\xi} = \left[\xi\ \xi_2\ \xi_3\right]^T$. In this case, because only an axial material flow is considered without any transverse flow, one has $s(\xi) \neq \xi$, $\xi_2 = s_2$ and $\xi_3 = s_3$ so that the only component of interest is ξ. The referential domain is depicted in Fig. 3.

From these considerations, Fig. 1 is simplified to Fig. 4. The material domain $\mathcal{L}_0$ is represented by the centerline coordinate s, the spatial domain $\mathcal{L}_t$ is represented by the curvilinear abscissa $x^\star$ of point P in the deformed configuration, and the referential domain $\mathcal{L}$ is represented by the scalar quantity ξ, understood as points of interest (or mesh nodes) lying on the centerline. The deformation gradients $\mathbf{F}$, $\bar{\mathbf{F}}$, $\widetilde{\mathbf{f}}$ are all represented by scalar quantities $F = \partial x^\star/\partial s$, $\bar{F} = \partial x^\star/\partial \xi$ and $\widetilde{f} = \partial s/\partial \xi$ that actually coincide with the Jacobians

$$J = F = \left\| \frac{\partial \mathbf{x}}{\partial s} \right\| = f^{-1} = j^{-1} \tag{17}$$

$$\bar{J} = \bar{F} = \left\| \frac{\partial \mathbf{x}}{\partial \xi} \right\| = \bar{j}^{-1} \tag{18}$$

$$\widetilde{j} = \widetilde{f} = \widetilde{J}^{-1} \tag{19}$$

Let the reader note that Eq. (5) still holds in this context. Indeed, one has

$$F = \left\| \frac{\partial \mathbf{x}}{\partial s} \right\| = \left(\frac{\partial s}{\partial \xi} \right)^{-1} \left\| \frac{\partial \mathbf{x}}{\partial \xi} \right\| = \widetilde{f}^{-1} \bar{F} \tag{20}$$

and, similarly,

$$f = \widetilde{f} \bar{F}^{-1} \tag{21}$$

as $\partial s/\partial \xi$ is a scalar quantity. Equations (20) and (21) will be extensively used throughout this paper in the calculus of variations, in order to express the deformation gradients with quantities defined on the referential domain.

In this paper, even though the Jacobians and the deformation gradients are equal, both notations will be kept. Notably, the deformation gradient will be used when a deformation measure is implied, whereas the Jacobian will be used when a change of domain or multiplicative factor is involved.

2.3 Equilibrium condition

In the quasistatic case, the equilibrium equation can be obtained from the virtual work principle that states that the variation

$$\delta \mathcal{W} = 0 \tag{22}$$

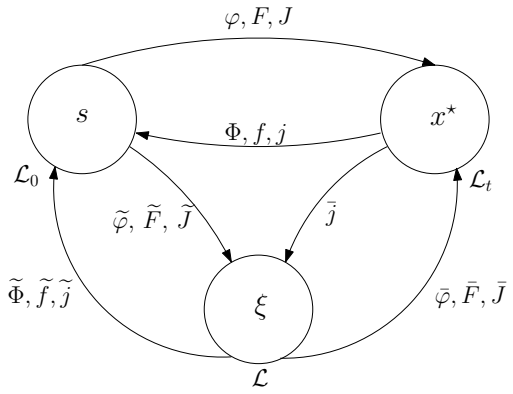

FIG. 4 – Material, spatial and referential domains with their mapping, deformation gradients and Jacobians in the case of a cable modeled as a unidimensional structure with a uniform distribution of strain in the cross section.

for all compatible virtual displacements, where $\mathcal{W}$ is the total potential energy $\mathcal{W} = \mathcal{W}^{\text{int}} + \mathcal{W}^{\text{ext}}$. The extension to the dynamic case can be obtained using Hamilton's principle. Defining $\mathcal{V}$ as the energy density per unit volume and under the assumption of a unidimensional structure with a uniform distribution of strains and material properties in the cross section, the virtual work can be rewritten as

$$\delta \left(A \int_{\mathcal{L}} \mathcal{V}\, dL \right) = 0 \tag{23}$$

where A is the cross-sectional area that is supposed to be constant along the cable span and dL is the length differential on the referential domain. The variation is expressed in the referential domain $\mathcal{L}$ and should be understood as a total variation, including the contribution of two distinct terms

$$\delta(\bullet) = \delta_{\mathbf{x}}(\bullet) + \delta_s(\bullet) \tag{24}$$

The equilibrium condition can then be written, according to the principle of virtual work, as

$$\delta(\mathcal{W}) = \delta_{\mathbf{x}}(\mathcal{W}) + \delta_s(\mathcal{W}) = 0 \tag{25}$$

The term $\delta_{\mathbf{x}}(\bullet)$ corresponds to the variation with respect to $\mathbf{x}$ keeping s fixed, i.e., it captures Lagrangian contributions resulting from the spatial motion. The term $\delta_s(\bullet)$ corresponds to the variation with respect to s keeping $\mathbf{x}$ fixed, i.e., it captures Eulerian contributions resulting from the material motion.

Although the previously defined energy density $\mathcal{V}$ is expressed in the referential domain, it can also be defined in the material domain as $\mathcal{V}_0$, or in the spatial domain as $\mathcal{V}_t$. To do so, it can be noted that, independently of the integration domain, the total potential energy of the cable should be the same:

$$\mathcal{W} = A \int_{\mathcal{L}} \mathcal{V}\, dL = A \int_{\mathcal{L}_0} \mathcal{V}_0\, dL_0 = A \int_{\mathcal{L}_t} \mathcal{V}_t\, dL_t \tag{26}$$

Using the previously defined Jacobians and relying on Fig. 4, the length differentials on the different domains are linked through the relation

$$dL = \widetilde{j}^{-1} dL_0 = \bar{J}^{-1} dL_t \tag{27}$$

As a consequence, using Eqs. (26) and (27), the energy densities in the different domains are related through the Jacobians as

$$\mathcal{V} = \widetilde{j}\mathcal{V}_0 = \bar{J}\mathcal{V}_t \tag{28}$$

2.4 Internal potential energy

Using the results of Section 2.2 and under the assumption of a linear stress-strain relation, the internal energy density for the cable expressed on the material domain is given as

$$\mathcal{V}_0^{\text{int}} = \frac{1}{2} E\, \varepsilon^2 \tag{29}$$

where E is Young's modulus.

For the spatial motion contribution, the variation of the internal energy is expressed keeping s fixed, with the implication that $\delta_{\mathbf{x}}\widetilde{f} = \delta_{\mathbf{x}}\widetilde{j} = 0$, so that $\delta_{\mathbf{x}}F = \delta_{\mathbf{x}}\bar{F}\,\widetilde{f}^{-1}$. This variation will describe the spatial motion at fixed material coordinates.

The variation is written as

$$\begin{aligned}
\delta_{\mathbf{x}}(\mathcal{W}^{\text{int}}) &= A\int_{\mathcal{L}} \delta_{\mathbf{x}}\mathcal{V}^{\text{int}} dL \\
&= A\int_{\mathcal{L}} \delta_{\mathbf{x}}\left(\widetilde{j}\mathcal{V}_0^{\text{int}}\right) dL \\
&= EA\int_{\mathcal{L}} \varepsilon\, \delta_{\mathbf{x}}\varepsilon\, \widetilde{j}\, dL \\
&= EA\int_{\mathcal{L}} \delta_{\mathbf{x}}\left(\frac{\partial \mathbf{x}}{\partial \xi}\right)^T \varepsilon\, \frac{\partial \mathbf{x}}{\partial \xi}\, \widetilde{j}^{-1}\, dL
\end{aligned} \tag{30}$$

since

$$\begin{aligned}
\delta_{\mathbf{x}}\bar{F} &= \delta_{\mathbf{x}}\left\|\frac{\partial \mathbf{x}}{\partial \xi}\right\| \\
&= \frac{1}{\bar{F}}\frac{\partial \mathbf{x}}{\partial \xi}^T \delta_{\mathbf{x}}\left(\frac{\partial \mathbf{x}}{\partial \xi}\right)
\end{aligned} \tag{31}$$

Equation (30) represents the first set of equilibrium equations.

For the material-motion contribution, the variation of the internal energy is expressed keeping $\mathbf{x}$ fixed, with the implication that $\delta_s\bar{F} = \delta_s\bar{J} = 0$, so that $\delta_s f = \delta_s\widetilde{f}\,\bar{F}^{-1}$. This variation will describe the material motion at fixed spatial coordinates.

The variation is written as

$$\begin{aligned}
\delta_s(\mathcal{W}^{\text{int}}) &= A\int_{\mathcal{L}} \delta_s\mathcal{V}^{\text{int}} dL \\
&= A\int_{\mathcal{L}} \delta_s\left(\widetilde{j}\mathcal{V}_0^{\text{int}}\right) dL \\
&= \frac{1}{2}EA\int_{\mathcal{L}} \left(\delta_s\widetilde{f}\varepsilon^2 + 2\,\widetilde{j}\,\varepsilon\,\delta_s\varepsilon\right) dL \\
&= \frac{1}{2}EA\int_{\mathcal{L}} \left(\delta_s\widetilde{f}\,\varepsilon^2 + 2\,\widetilde{j}\,\varepsilon\,F\,\bar{F}\,\delta_s\widetilde{f}^{-1}\right) dL \\
&= \frac{1}{2}EA\int_{\mathcal{L}} \delta_s\widetilde{f}\left(\varepsilon^2 - 2\,F^2\,\varepsilon\right) dL
\end{aligned} \tag{32}$$

Equation (32) gives the second set of equilibrium equations.

In order to solve the equilibrium equations (30) and (32), a popular option is to work with an iterative scheme such as a Newton scheme, so that the equilibrium equations need to be linearized. As two mappings are present, the linearizations must be alternately computed with respect to one variable while keeping the other fixed, hence

$$\Delta\delta(\bullet) = \Delta_{\mathbf{x}}\delta_{\mathbf{x}}(\bullet) + \Delta_{\mathbf{x}}\delta_s(\bullet) + \Delta_s\delta_{\mathbf{x}}(\bullet) + \Delta_s\delta_s(\bullet) \tag{33}$$

The linearizations are written as

$$\Delta_{\mathbf{x}}\delta_{\mathbf{x}}(\mathcal{W}^{\text{int}}) = EA\int_{\mathcal{L}} \delta_{\mathbf{x}}\left(\frac{\partial \mathbf{x}}{\partial \xi}\right)^T \left(\varepsilon\,\mathbf{I}\,\widetilde{j}^{-1} + \frac{\partial \mathbf{x}}{\partial \xi}\,\frac{\partial \mathbf{x}^T}{\partial \xi}\,\widetilde{j}^{-3}\right)\Delta_{\mathbf{x}}\frac{\partial \mathbf{x}}{\partial \xi}\,dL \tag{34}$$

$$\Delta_s\delta_s(\mathcal{W}^{\text{int}}) = EA\int_{\mathcal{L}} \delta_s\widetilde{f}\left(\varepsilon\,F^3 + F^5\right)\,\bar{J}^{-1}\,\Delta_s\widetilde{f}\,dL \tag{35}$$

$$\Delta_{\mathbf{x}}\delta_s(\mathcal{W}^{\text{int}}) = -EA\int_{\mathcal{L}} \delta_s\widetilde{f}\left(\varepsilon + F^2\right)\widetilde{j}^{-2}\,\frac{\partial \mathbf{x}^T}{\partial \xi}\,\Delta_{\mathbf{x}}\frac{\partial \mathbf{x}}{\partial \xi}\,dL \tag{36}$$

$$\Delta_s\delta_{\mathbf{x}}(\mathcal{W}^{\text{int}}) = -EA\int_{\mathcal{L}} \delta_{\mathbf{x}}\left(\frac{\partial \mathbf{x}}{\partial \xi}\right)^T \frac{\partial \mathbf{x}}{\partial \xi}\left(\varepsilon + F^2\right)\,\widetilde{j}^{-2}\,\Delta_s\widetilde{f}\,dL \tag{37}$$

where it can be seen from Eqs. (36) and (37) that the tangent stiffness matrix will be symmetric.

2.5 External loading

The contribution of external loading can be added to the equilibrium equations. In what follows, both cases of distributed loading and punctual loading will be successively studied.

First, a distributed loading with an external work density of the form $\mathcal{V}_0^{\text{ext}} = -\mathbf{x}^T\mathbf{b}_0$ is considered, where $\mathbf{b}_0$ is the vector of external forces per unit length expressed in the inertial frame. It is first assumed that $\mathbf{b}_0$ could explicitly depend on the material coordinate s. Similarly as in the previous sections, the virtual work done by the external forces is expressed as

$$\delta(\mathcal{W}^{\text{ext}}) = \int_{\mathcal{L}} \delta\mathcal{V}_0^{\text{ext}}\widetilde{j}\,dL \tag{38}$$

One should be careful that $\mathbf{x} = \bar{\boldsymbol{\varphi}}(\xi)$ is evaluated on the referential domain and has therefore no explicit dependence on the material coordinate s. In this section, the representation of the virtual displacements as $\delta_{\mathbf{x}}\bar{\boldsymbol{\varphi}}$ and $\delta_s\widetilde{\Phi}$ is kept, instead of $\delta_{\mathbf{x}}\mathbf{x}$ and $\delta_s s$, to highlight the fact that they capture virtual spatial and material displacements with respect to the referential domain.

The virtual work for the spatial motion is obtained as

$$\delta_{\mathbf{x}}(\mathcal{W}^{\text{ext}}) = -\int_{\mathcal{L}} \delta_{\mathbf{x}}\bar{\boldsymbol{\varphi}}^T\mathbf{b}_0\,\widetilde{j}\,dL \tag{39}$$

and the virtual work for the material motion as

$$\delta_s(\mathcal{W}^{\text{ext}}) = -\int_{\mathcal{L}} \left(\delta_s\widetilde{j}\,\mathbf{x}^T\mathbf{b}_0 + \widetilde{j}\,\mathbf{x}^T\frac{\partial \mathbf{b}_0}{\partial s}\delta_s\widetilde{\Phi}\right)dL \tag{40}$$

Equation (40) represents so-called material or configurational forces, which have already been studied e.g., by Eshelby [10,28,30]. The second term in the integral takes into account the fact that the loading $\mathbf{b}_0$ depends on s and could be distributed on a portion of the material domain

only. In the special case where the external force is uniformly distributed over the cable, $\mathbf{b}_0$ is independent of s, so that Eq. (40) becomes:

$$\delta_s(\mathcal{W}^{\text{ext}}) = -\int_{\mathcal{L}} \delta_s \widetilde{f}\, \mathbf{x}^T \mathbf{b}_0 \, dL \tag{41}$$

Secondly, in the case where a load is punctually applied at a location $\xi^\star \in [0, L]$, one has

$$\delta(\mathcal{W}^{\text{ext}}) = \delta(\mathcal{W}_0^{\text{ext}}) = -\delta\boldsymbol{\varphi}^T|_{\xi^\star}\, \mathbf{t}_0 \tag{42}$$

where $\mathbf{t}_0$ is the vector of external punctual loads applied at point $\xi^\star$. This means that the point of application of the load is fixed at the position $\xi^\star$ in the referential domain, and that both spatial and material motions may occur at that position. The total variation of $\boldsymbol{\varphi} = \bar{\boldsymbol{\varphi}} \circ \widetilde{\varphi}$ should thus be taken into account using Eq. (24)

$$\begin{aligned} \delta\boldsymbol{\varphi} &= \delta_{\mathbf{x}}\boldsymbol{\varphi} + \delta_s\boldsymbol{\varphi} \\ &= \delta_{\mathbf{x}}\bar{\boldsymbol{\varphi}} + \frac{\partial\bar{\boldsymbol{\varphi}}}{\partial\xi}\, \delta_s\widetilde{\varphi} \end{aligned} \tag{43}$$

and using the mapping identity

$$\widetilde{\varphi}(\widetilde{\Phi}) = 1 \tag{44}$$

$$\Leftrightarrow \delta\widetilde{\varphi} + \widetilde{j}^{-1}\, \delta\widetilde{\Phi} = 0 \tag{45}$$

Equation (42) is rewritten as

$$\delta_{\mathbf{x}}(\mathcal{W}^{\text{ext}}) = -\delta_{\mathbf{x}}\bar{\boldsymbol{\varphi}}^T|_{\xi^\star}\, \mathbf{t}_0 \tag{46}$$

and

$$\delta_s(\mathcal{W}^{\text{ext}}) = \delta_s\widetilde{\Phi}|_{\xi^\star}\, \frac{\partial\mathbf{x}^T}{\partial\xi}\, \mathbf{t}_0\, \widetilde{j}^{-1} \tag{47}$$

It should be noted that the contribution of Eq. (46) is zero if the spatial motion is prevented at point $\xi^\star$, as $\delta_{\mathbf{x}}\bar{\boldsymbol{\varphi}}|_{\xi^\star}$ will become zero. This is notably the case when the force is applied at a fixed spatial location. On the other hand, the contribution in Eq. (47) becomes zero if no flow is allowed at point $\xi^\star$, e.g., if the force is always applied at the same material particle. This is also particularly the case at the extremities of the cable, where the no-flow boundary conditions will enforce $\delta_s\widetilde{\Phi}|_0 = \delta_s\widetilde{\Phi}|_L = 0$.

Unfortunately, the gradient $\partial\mathbf{x}/\partial\xi$ and the Jacobian $\widetilde{j}$ in Eq. (47) are discontinuous at point $\xi^\star$ due to the punctual nature of the applied loading so that this equation cannot be used as such. This problem was investigated in detail in [19], where it is demonstrated that the gradient and the Jacobian should actually be replaced by the arithmetic mean of their two values across the discontinuity.

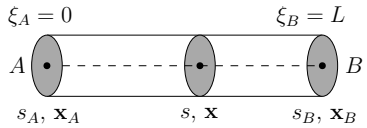

FIG. 5 – Cable element. The variables s and $\mathbf{x}$ are interpolated between the nodal values s_A and s_B and $\mathbf{x}_A$ and $\mathbf{x}_B$, respectively, with linear shape functions of ξ.

3 Finite element discretization

A finite element with two nodes A and B and linear shape functions is proposed in the following, as depicted in Fig. 5. Initially, the reference domain is equal to the material domain, so that $\xi_A = s_A = 0$ and $\xi_B = s_B = L$, where L is the undeformed length of the cable. However, after motion, s_A is not necessarily equal to ξ_A and s_B is not necessarily equal to ξ_B, as a flow of material can arise between the elements. The nodal value of the unknown mappings $s = \widetilde{\Phi}$ and $\mathbf{x} = \bar{\boldsymbol{\varphi}}$ will be denoted using the following vectors

$$\mathbf{q}_s(t) = \begin{bmatrix} s_A(t) \\ s_B(t) \end{bmatrix} \tag{48}$$

$$\mathbf{q}_{\mathbf{x}}(t) = \begin{bmatrix} \mathbf{x}_A(t) \\ \mathbf{x}_B(t) \end{bmatrix} \tag{49}$$

and the vector of coordinates of the element is simply

$$\mathbf{q}(t) = \begin{bmatrix} \mathbf{q}_s(t) \\ \mathbf{q}_{\mathbf{x}}(t) \end{bmatrix} \tag{50}$$

Over the element, the values of the maps can be approximated using linear shape functions

$$\widetilde{\Phi}(\xi, t) = \mathbf{N}_s(\xi)\, \mathbf{q}_s(t) \tag{51}$$

and

$$\bar{\boldsymbol{\varphi}}(\xi, t) = \mathbf{N}_{\mathbf{x}}(\xi)\, \mathbf{q}_{\mathbf{x}}(t) \tag{52}$$

with

$$\mathbf{N}_s(\xi) = \begin{bmatrix} N_1(\xi) & N_2(\xi) \end{bmatrix} \tag{53}$$

and

$$\mathbf{N}_{\mathbf{x}}(\xi) = \begin{bmatrix} N_1(\xi) & 0 & 0 & N_2(\xi) & 0 & 0 \\ 0 & N_1(\xi) & 0 & 0 & N_2(\xi) & 0 \\ 0 & 0 & N_1(\xi) & 0 & 0 & N_2(\xi) \end{bmatrix} \tag{54}$$

where $N_1 = (1 - \xi)/L$ and $N_2 = \xi/L$ are functions of $\xi \in [0, L]$.

The derivatives of the mappings are defined as

$$\frac{\partial \widetilde{\Phi}}{\partial \xi} = \widetilde{f} = \mathbf{B}_s\, \mathbf{q}_s \tag{55}$$

and

$$\frac{\partial \bar{\boldsymbol{\varphi}}}{\partial \xi} = \frac{\partial \mathbf{x}}{\partial \xi} = \mathbf{B}_{\mathbf{x}}\, \mathbf{q}_{\mathbf{x}} \tag{56}$$

with

$$\mathbf{B}_s = \begin{bmatrix} \dfrac{\partial N_1}{\partial \xi} & \dfrac{\partial N_2}{\partial \xi} \end{bmatrix} \tag{57}$$

and

$$\mathbf{B}_{\mathbf{x}} = \begin{bmatrix} \dfrac{\partial N_1}{\partial \xi} & 0 & 0 & \dfrac{\partial N_2}{\partial \xi} & 0 & 0 \\ 0 & \dfrac{\partial N_1}{\partial \xi} & 0 & 0 & \dfrac{\partial N_2}{\partial \xi} & 0 \\ 0 & 0 & \dfrac{\partial N_1}{\partial \xi} & 0 & 0 & \dfrac{\partial N_2}{\partial \xi} \end{bmatrix} \tag{58}$$

where $\partial N_1/\partial \xi = -1/L$ and $\partial N_2/\partial \xi = 1/L$

Since $\mathbf{B}_s$ and $\mathbf{B}_{\mathbf{x}}$ are constant, one has

$$\delta_s \widetilde{f} = \mathbf{B}_s\, \delta_s \mathbf{q}_s \tag{59}$$

and

$$\delta_{\mathbf{x}} \left(\frac{\partial \mathbf{x}}{\partial \xi} \right) = \mathbf{B}_{\mathbf{x}}\, \delta_{\mathbf{x}} \mathbf{q}_{\mathbf{x}} \tag{60}$$

3.1 Internal force vector

Using the previously defined quantities, in its discretized form, Eq. (30) becomes

$$\delta_{\mathbf{x}}(\mathcal{W}^{\text{int}}) = EA\, \delta_{\mathbf{x}} \mathbf{q}_{\mathbf{x}}^T \int_{\mathcal{L}} \mathbf{B}_{\mathbf{x}}^T\, \varepsilon\, \mathbf{B}_{\mathbf{x}}\, \mathbf{q}_{\mathbf{x}}\, (\mathbf{B}_s\, \mathbf{q}_s)^{-1} dL \tag{61}$$

with $\varepsilon = \frac{1}{2}\left(F^2 - 1\right)$ and $F = \|\mathbf{B}_{\mathbf{x}}\, \mathbf{q}_{\mathbf{x}}\|\, (\mathbf{B}_s\, \mathbf{q}_s)^{-1}$. For linear shape functions, the integration over the element length L is trivial:

$$\delta_{\mathbf{x}}(\mathcal{W}^{\text{int}}) = EA\, L\, \delta_{\mathbf{x}} \mathbf{q}_{\mathbf{x}}^T\, \mathbf{B}_{\mathbf{x}}^T\, \varepsilon\, \mathbf{B}_{\mathbf{x}}\, \mathbf{q}_{\mathbf{x}}\, (\mathbf{B}_s\, \mathbf{q}_s)^{-1} \tag{62}$$

For the material motion contribution, Eq. (32) becomes

$$\delta_s(\mathcal{W}^{\text{int}}) = \frac{1}{2} EA\, \delta_s \mathbf{q}_s^T \int_{\mathcal{L}} \left(\varepsilon^2 - 2\, F^2\, \varepsilon\right) dL \tag{63}$$

Again, with the use of linear shape functions, the integration over the length L of the current element is trivial:

$$\delta_s(\mathcal{W}^{\text{int}}) = \frac{1}{2}\, EA\, L \delta_s \mathbf{q}_s^T \left(\varepsilon^2 - 2\, F^2\, \varepsilon\right) \tag{64}$$

We obtain

$$\delta_{\mathbf{x}}(\mathcal{W}^{\text{int}}) + \delta_s(\mathcal{W}^{\text{int}}) = \delta \mathbf{q}^T\, \mathbf{f}^{\text{int}} \tag{65}$$

with

$$\mathbf{f}^{\text{int}} = EA\, L \begin{bmatrix} \dfrac{1}{2} \mathbf{B}_s^T \left(\varepsilon^2 - 2\, F^2\, \varepsilon\right) \\ \mathbf{B}_{\mathbf{x}}^T\, \mathbf{B}_{\mathbf{x}}\, \mathbf{q}_{\mathbf{x}}\, (\mathbf{B}_s\, \mathbf{q}_s)^{-1}\, \varepsilon \end{bmatrix} = \begin{bmatrix} \mathbf{f}_{\text{mat}}^{\text{int}} \\ \mathbf{f}_{\text{spatial}}^{\text{int}} \end{bmatrix} \tag{66}$$

3.2 External force vector

For a uniformly distributed external loading over the material domain, the discretization of Eqs. (39) and (41) is written as

$$\delta_{\mathbf{x}}(\mathcal{W}^{\text{ext}}) = -\int_{\mathcal{L}} \delta_{\mathbf{x}}\mathbf{q}_{\mathbf{x}}^T\,\mathbf{N}_{\mathbf{x}}^T\,\mathbf{b}_0\,\mathbf{B}_s\,\mathbf{q}_s\,dL \tag{67}$$

and

$$\delta_s(\mathcal{W}^{\text{ext}}) = -\int_{\mathcal{L}} \delta_s\mathbf{q}_s^T\,\mathbf{B}_s^T\,\mathbf{q}_{\mathbf{x}}^T\,\mathbf{N}_{\mathbf{x}}^T\,\mathbf{b}_0\,dL \tag{68}$$

For an external punctual loading at $\xi^\star$, the discretization of Eqs. (46) and (47) yields

$$\delta_{\mathbf{x}}(\mathcal{W}^{\text{ext}}) = -\delta_{\mathbf{x}}\mathbf{q}_{\mathbf{x}}^T\,\mathbf{N}_{\mathbf{x}}(\xi^\star)^T\,\mathbf{t}_0 \tag{69}$$

and

$$\delta_s(\mathcal{W}^{\text{ext}}) = \delta_s\mathbf{q}_s^T\,\mathbf{N}_s(\xi^\star)^T\,\overline{\mathbf{q}_{\mathbf{x}}^T\mathbf{B}_{\mathbf{x}}^T}\,\mathbf{t}_0\,\overline{(\mathbf{B}_s\mathbf{q}_s)}^{-1} \tag{70}$$

where $\mathbf{N}_{\mathbf{x}}(\xi^\star)$ and $\mathbf{N}_s(\xi^\star)$ are the shape functions evaluated at $\xi^\star$ and where $\overline{\mathbf{q}_{\mathbf{x}}^T\mathbf{B}_{\mathbf{x}}^T}$ and $\overline{(\mathbf{B}_s\mathbf{q}_s)}$ are the arithmetic means between their values before and after $\xi^\star$. In this specific case, the vector of external forces becomes

$$\mathbf{f}^{\text{ext}} = \begin{bmatrix} \mathbf{N}_s(\xi^\star)^T\,\overline{\mathbf{q}_{\mathbf{x}}^T\mathbf{N}_{\mathbf{x}}^T}\,\mathbf{t}_0\,\overline{(\mathbf{B}_s\mathbf{q}_s)}^{-1} \\ -\mathbf{N}_{\mathbf{x}}(\xi^\star)^T\,\mathbf{t}_0 \end{bmatrix} = \begin{bmatrix} \mathbf{f}_{\text{mat}}^{\text{ext}} \\ \mathbf{f}_{\text{spatial}}^{\text{ext}} \end{bmatrix} \tag{71}$$

3.3 Discretized equilibrium equations

The modeling of multibody systems often involves constraints. In the present ALE formulation, constraints can be applied to the material coordinates, for instance, to impose the zero-flow boundary conditions, or to the spatial coordinates, e.g. to enforce a fixed position, a bilateral link between the cable mesh and a rigid body or a driven motion for one or several nodes of the mesh in space. It should be noted that it is perfectly possible to enforce constraints on both the material and spatial coordinates of the same node, for example, a node with a prescribed kinematic motion through which no flow of material can occur. Moreover, the formulation of the cable could be coupled to any multibody system involving its own constraints, e.g., to model rigid links or joints. The vector of constraints can thus be noted as

$$\mathbf{g}(\mathbf{q}) = \begin{bmatrix} \mathbf{g}_{\text{mat}}(\mathbf{q}_s) \\ \mathbf{g}_{\text{spatial}}(\mathbf{q}_{\mathbf{x}}) \end{bmatrix} = \mathbf{0} \tag{72}$$

The equilibrium of the system in the quasistatic case is then written as

$$\begin{aligned} \mathbf{f}^{\text{int}} + \mathbf{f}^{\text{ext}} + \mathbf{G}^T\boldsymbol{\lambda} &= \mathbf{0} \\ \mathbf{g}(\mathbf{q}) &= \mathbf{0} \end{aligned} \tag{73}$$

where $\mathbf{G}$ is the constraint gradient with respect to the generalized coordinates $\mathbf{q}$.

The residue can be defined from the equilibrium equations as

$$\mathbf{r} = \begin{bmatrix} \mathbf{f}_{\text{mat}}^{\text{int}} + \mathbf{f}_{\text{mat}}^{\text{ext}} + \mathbf{G}_{\text{mat}}^T\boldsymbol{\lambda}_{\text{mat}} \\ \mathbf{f}_{\text{spatial}}^{\text{int}} + \mathbf{f}_{\text{spatial}}^{\text{ext}} + \mathbf{G}_{\text{spatial}}^T\boldsymbol{\lambda}_{\text{spatial}} \\ \mathbf{g}(\mathbf{q}) \end{bmatrix} = \begin{bmatrix} \mathbf{r}_{\text{mat}} \\ \mathbf{r}_{\text{spatial}} \\ \mathbf{r}_{\mathbf{g}} \end{bmatrix} \tag{74}$$

where we define $\mathbf{G}_{\text{mat}}$ and $\mathbf{G}_{\text{spatial}}$ as the constraint gradients $\partial\mathbf{g}_{\text{mat}}/\partial\mathbf{q}_s$ and $\partial\mathbf{g}_{\text{spatial}}/\partial\mathbf{q}_{\mathbf{x}}$, respectively.

3.4 Regularization of the problem

In a purely Lagrangian setting i.e., when no flow of material is allowed through the nodes, the spatial solution $\mathbf{x}$ will be the one that minimizes the potential energy for the chosen values of the material coordinates s of the mesh. This means that, around a stable solution, a purely Lagrangian description leads to a positive-definite tangent stiffness matrix of the internal and external forces, which ensures the convergence of the Newton solver.

However, if the no-flow constraint is relaxed, as it is the case in an ALE formulation, the equations are obtained from the variation of the potential energy with respect to the two variables s and $\mathbf{x}$. Consequently, the solution will be such that the material and spatial coordinates represent a stationary point of the potential energy. If the problem is convex, the mesh is called "energy optimal" [2]. This property will be studied in a numerical example in the following section. Nevertheless, when the material flow with respect to the mesh is also allowed, several problems can arise, as identified in [29]. First, the uniqueness of the solution is not guaranteed. Indeed, there might be several node configurations for the same spatial solution with the same potential energy, for instance, when the strain field is uniform along the whole cable span. The discretized energy is thus insensitive to the material position of the nodes on the cable so that there exists an infinity of solutions that satisfy the minimum-energy condition. Secondly, at an undeformed configuration, the tangent stiffness matrix is singular and thus not positive-definite. Finally, even in the unconstrained case, the tangent stiffness matrix can have negative eigenvalues, indicating a nonconvexity of the problem. Local convexity is usually recovered in the neighborhood of the solution. In [2], dynamic constraints are introduced to eliminate the material coordinates having a zero residual at each iteration. Although this method solves the case where the tangent stiffness matrix is singular, it does not necessarily improve the convexity of the problem. In [29], a regularization technique is applied to the whole material problem.

In this paper, this regularization is modified as follows. At each load step n, two regularized subproblems are solved consecutively.

- In the first subproblem, a constant term is added to the material part of the residual as

$$\mathbf{r}_{\text{mat}}^{n\star} := \mathbf{r}_{\text{mat}}^{n} + 2\alpha(\mathbf{q}_s^{n\star} - \mathbf{q}_s^{n-1}) \tag{75}$$

  so that the material part of the tangent stiffness $\mathbf{S}_{\text{mat}}$ takes the expression

$$\mathbf{S}_{\text{mat}}^{n\star} := \mathbf{S}_{\text{mat}}^{n} + 2\alpha\mathbf{I} \tag{76}$$

  where α is a positive constant whose role is to force this part of the tangent stiffness to be positive-definite. This resolves the nonconvexity of the problem and the Newton solver will converge to a solution $\mathbf{q}^{n\star}$. However, it can be noted that the term $2\alpha(\mathbf{q}_s^{n\star} - \mathbf{q}_s^{n-1})$ can be nonnegligible, so that the obtained solution $\mathbf{q}^{n\star}$ is not a solution of the unregularized problem.
- The second subproblem is formulated to solve the previously identified issue. In our experience, the configuration $\mathbf{q}^{n\star}$ is sufficiently close to the unregularized solution so that the unregularized tangent stiffness of the internal and external forces does not have any negative eigenvalue. However, the uniqueness of the solution is still not guaranteed, implying that some lines of the tangent stiffness can be dependent. At each iteration, the dependent lines of the tangent stiffness matrix are identified through its QR decomposition, and the rank deficiency of the resulting permutation matrix is examined. Since the decomposition is performed on the entire tangent stiffness matrix, some dependent lines may correspond to spatial coordinates, while others may correspond to material coordinates. To obtain a unique set of dependent lines that correspond exclusively to material coordinates, the dependent lines associated with spatial coordinates are swapped with their material counterparts, as each spatial coordinate

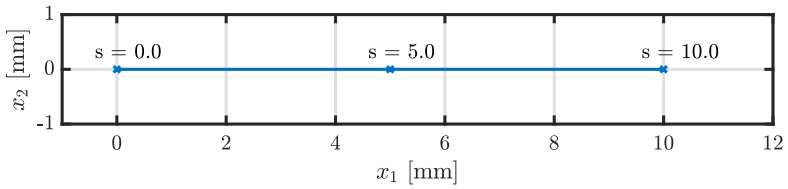

(a) Initial position.

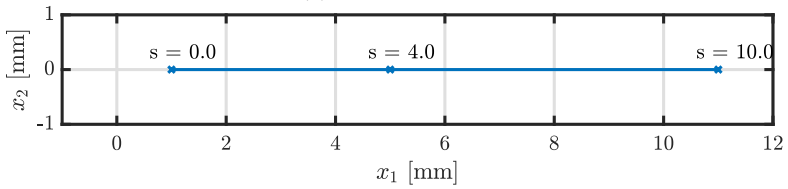

(b) Final position.

FIG. 6 – Material flow through the fixed middle node due to the bar translation.

has a unique corresponding material coordinate. In this way, the selection of dependent lines is such that it only includes indices of material coordinates. In the second subproblem, the regularization is then applied exclusively to the corresponding components of the material part of the residual as

$$\mathbf{r}^{n\star\star}_{\text{mat, dependent}} := \mathbf{r}^{n}_{\text{mat, dependent}} + 2\alpha(\mathbf{q}^{n}_{s,\text{dependent}} - \mathbf{q}^{n\star}_{s,\text{dependent}}) \tag{77}$$

The material part of the tangent stiffness is modified accordingly

$$\mathbf{S}^{n\star\star}_{\text{mat,dependent}} := \mathbf{S}^{n}_{\text{mat,dependent}} + 2\alpha\mathbf{I} \tag{78}$$

The Newton solver starts from the initial guess $\mathbf{q}^{n\star}$ and converges to the final solution $\mathbf{q}^{n}$ of the load step n. It should be noted that this regularization does not alter the solution, as was the case for the first subproblem. Indeed, the regularization term $2\alpha(\mathbf{q}^{n}_{s,\text{dependent}} - \mathbf{q}^{n\star}_{s,\text{dependent}})$ only acts on the dependent solution components and can be seen as a kind of quasistatic damping. Among the nonunique solutions of the unregularized problem, it penalizes the ones departing from $\mathbf{q}^{n\star}_{s,\text{dependent}}$ so that the final solution satisfies $\mathbf{q}^{n}_{s,\text{dependent}} = \mathbf{q}^{n\star}_{s,\text{dependent}}$.

4 Numerical results

4.1 Bar with simple material flow

In order to illustrate the formulation, a simple example is first studied. It consists in the quasistatic rigid-body motion of a 3-node 10-mm-long bar in the axial direction. The same displacement of 1 mm is imposed on both end nodes in a single step. A no-flow boundary condition is imposed on the material coordinate at the two extremities. The middle node is completely fixed in space. These conditions are all imposed through the constraint vector $\mathbf{g}$. The material is allowed to flow through the middle node, as its material coordinate is left unconstrained. The aim is to check that the observed material flow is consistent with the imposed translation of the bar. No regularization of the problem is needed in this context as there is only one free coordinate. As can be seen in Fig. 6, in the final configuration, the material coordinate of the particle at the middle node has been shifted by 1 mm, which agrees with the amplitude of the translation.

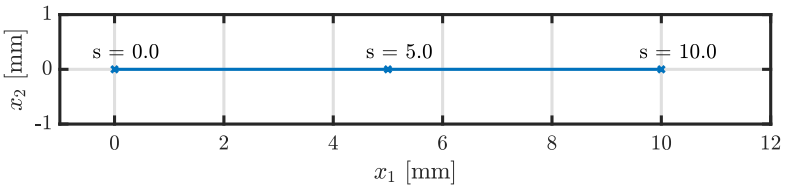

(a) Middle node with initial coordinates $s = 5$ mm and $x_1 = 5$ mm.

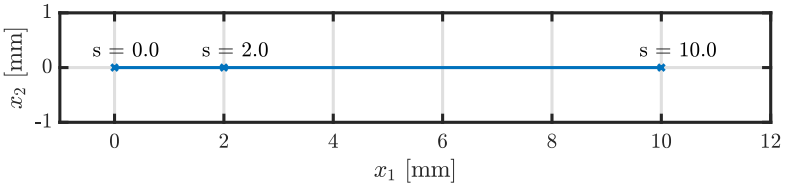

(b) Middle node with initial coordinates $s = 2$ mm and $x_1 = 2$ mm.

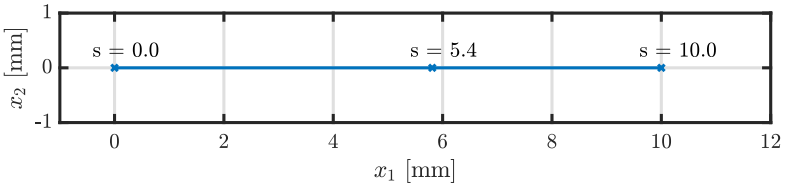

(c) Final configuration for both initial configurations.

FIG. 7 – The solution for the axially uniformly loaded cable is an optimal mesh regardless of the initial middle-node position.

4.2 Clamped-clamped cable under constant axial distributed loading

This example is inspired by [2] and is intended to show the possibility to apply a distributed load on the cable and the mesh-optimality property mentioned in Section 3.4. A cable, with material properties $E = 1$ GPa, cross-sectional area $A = \pi$ mm^2 and a length $L = 10$ mm, is clamped at both extremities and a uniform axial distributed loading $b_0 = 100000$ N/m is applied on the cable span. The cable is divided into two elements, so that only the middle node, with initial coordinates $s = 5$ mm and $x_1 = 5$ mm, is free to move both spatially and materially. At the undeformed configuration, the tangent stiffness matrix is singular. In this context, the proposed regularization is applied with $\alpha = 100$. With 40 load steps, the average number of Newton iterations for the first and second regularized subproblems is 2.13 and 1.5, respectively.

For this particular example, the 1D equations that need to be solved are two scalar equations for the two unknown axial coordinates of the middle node B denoted s_B and x_B

$$\begin{cases} \dfrac{1}{4}EA\left(\dfrac{3}{2}\left(F_2^4 - F_1^4\right) + F_1^2 - F_2^2\right) + b_0\dfrac{x_C - x_A}{2} = 0 \\ \dfrac{1}{2}EA\left(F_1^3 - F_2^3 + F_2 - F_1\right) - b_0\dfrac{s_C - s_A}{2} = 0 \end{cases} \tag{79}$$

where the material and spatial coordinates of the clamped nodes s_A, s_C, x_A and x_C are fixed to their initial values and where

$$F_1 = \frac{x_B - x_A}{s_B - s_A},\ F_2 = \frac{x_C - x_B}{s_C - s_B} \tag{80}$$

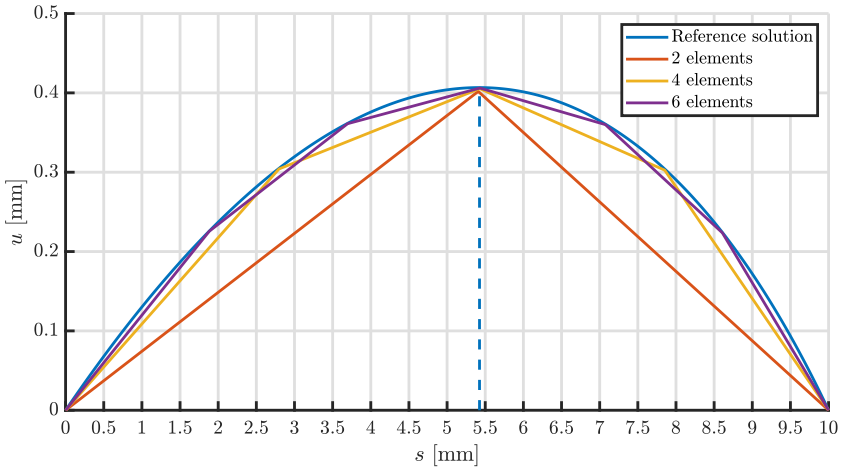

FIG. 8 – Displacement u as a function of the material position s for the axially uniformly loaded clamped-clamped cable for several numbers of ALE elements. The reference solution is obtained from a purely Lagrangian simulation with 800 elements.

The results are presented in Fig. 7. It is observed that the middle node moves towards the right while the material flow is directed to the left, such that its final coordinates are $s = 5.41$ mm and $x_1 = 5.81$ mm.

In Fig. 8, this result can be compared to a reference solution of the displacement field u as a function of the material coordinate s obtained with a finely discretized mesh in a purely Lagrangian setting. It is remarkable that the material position obtained in the previous simulation coincides with the material coordinates for which the displacement u reaches its maximum. By increasing the number of ALE elements, it can also be seen in Fig. 8 that the exact displacement field is approached with few elements. This illustrates the fact that the mesh becomes optimal energy-wise. One can confirm the energy optimality by plotting the potential energy $\mathcal{W} = \mathcal{W}_{\text{int}} + \mathcal{W}_{\text{ext}}$ as a function of the material position of the middle node in a purely Lagrangian setting with two elements, see Fig. 9. It can be appreciated that the minimum of the potential energy is achieved when the position of the middle node is chosen as $s = 5.41$ mm, which is the solution given by the ALE simulation. It can also be checked that the same solution is recovered by the ALE formulation regardless of the initial middle-node position, e.g., when the initial position of the middle node is changed to $s = 2$ mm and $x_1 = 2$ mm as shown in Fig. 7.

4.3 Cable-pulley system

4.3.1 Frictionless cable

In this example, a cable-pulley system will be studied. The aim is to model the system when sufficient tension is assumed in the cable, so that closed contact is achieved between the cable and the pulley without any gap. It is considered that the contact region of the cable on the pulley is known *a priori*. In such cases, as previously mentioned, the drawback of a purely Lagrangian formulation for a cable-pulley system is that the discretization of the cable should be fine enough over the whole length to represent the contact and friction between the pulley and the cable during the sliding motion of the cable. In contrast, an ALE formulation may only require small

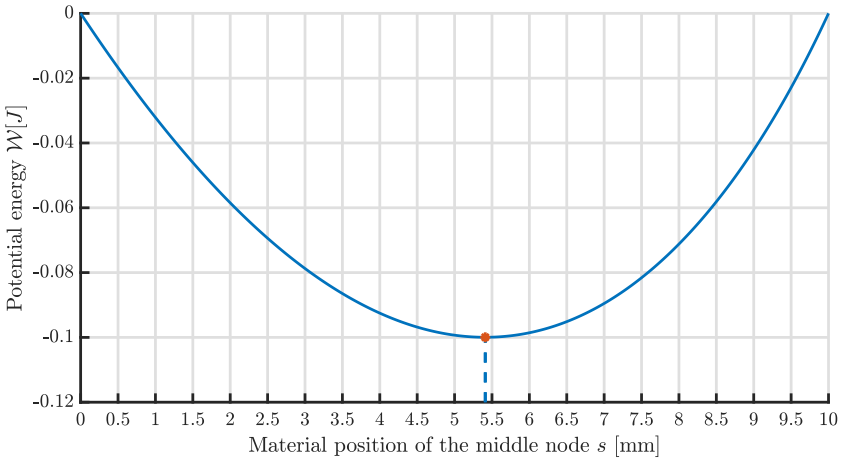

FIG. 9 – Potential energy $\mathcal{W}$ as a function of the material position s of the middle-node for the axially uniformly loaded clamped-clamped cable in a purely Lagrangian setting with two finite elements. A minimum is reached for $s = 5.41$ mm.

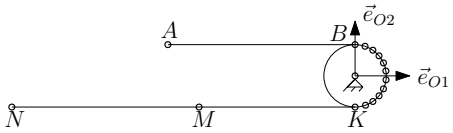

FIG. 10 – ALE discretization of the cable in a cable-pulley system.

elements in the contact zone between the cable and the pulley while the rest of the cable is modeled using coarser elements, as depicted in Fig. 10. For the nodes in the contact zone, a flow of material is thus observed.

The numerical simulation consists in a planar and frictionless cable-pulley system where the pulley center is fixed, the rotation of the pulley is blocked and an imposed displacement is applied to the end nodes of the cable in several steps. In order to show the possibility to take into account the elasticity of the cable, a larger displacement is imposed at one of the two ends: $\Delta x_{A,1} = 10$ mm at the top extremity in the positive x-direction and $\Delta x_{N,1} = 20$ mm at the bottom extremity in the negative x_1-direction, whereas their motion in the x_2- and x_3-directions is not allowed. Again, a no-flow boundary condition is applied at the two extremities. All the nodes in contact with the pulley are constrained to keep their spatial position. In this case, there is no need for generalized coordinates to represent the pulley, as its rotation is blocked. The node M, located between the end of the cable and the pulley, initially at $s_M = 256.9$, is not allowed to move in the x_2- and x_3-directions but is unconstrained in the x_1-direction. In this example, the cable has an initial length $L = 306.9$ mm, a Young's modulus $E = 3$ GPa, a cross-sectional area $A = 7.069$ mm^2, and the pulley has a radius $R = 50$ mm. The regularization parameter α has been set to 1. The results are presented in Fig. 11.

It can be observed in Fig. 11b that the spatially constrained nodes see a flow of material through them, as expected. Indeed, the material value s decreases with time, indicating that the nodes do not follow the same material particle during the simulation. On the other hand, the end nodes always follow the material particles located at $s = 0$ and $s = L$, because of the imposed boundary conditions. Finally, it can be noted that node M keeps a fixed material position at

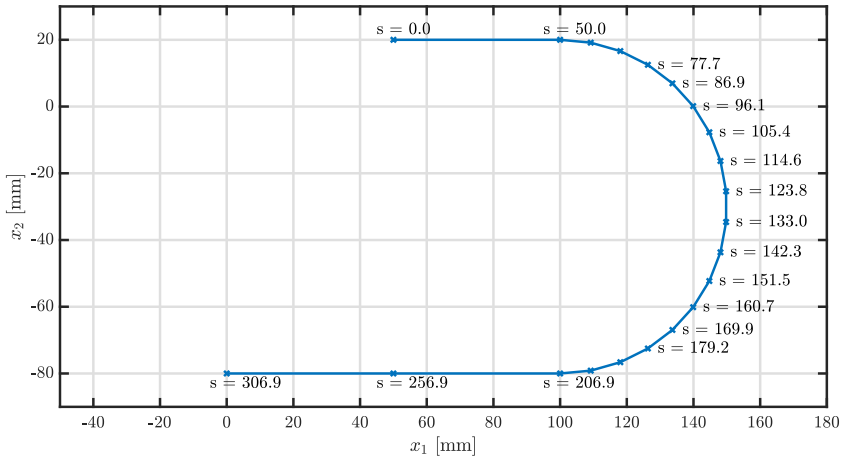

(a) Initial configuration.

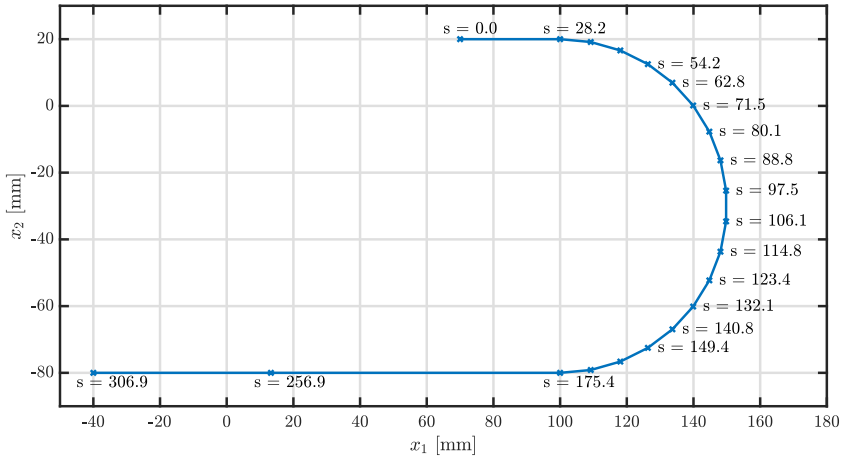

(b) Final configuration.

FIG. 11 – Simulation of the cable-pulley system with imposed displacements on both ends.

$s = 256.9$ mm during the whole simulation. As mentioned in Section 3.4, the solution for the material coordinate of this node is not unique because there is a constant strain in the last two elements. This can be seen in Fig. 12 representing the strain as a function of s. This means that each value of s between $s_K = 175.4$ mm and $s_N = L$ is a solution to this nonconvex minimization problem. In other words, the solution is independent of the material coordinate of this node. As previously mentioned, with the help of the proposed regularization, the Newton solver forces this node to converge to its initial material coordinate among all the possible solutions. The average number of Newton iterations for the first regularized subproblem is 4, and 1 for the second subproblem, with 20 load steps.

4.3.2 Introducing friction

In order to take into account the friction between the cable and the pulley, a friction law can be applied to each node in contact with the pulley. Relying on Fig. 10, these nodes are all the nodes

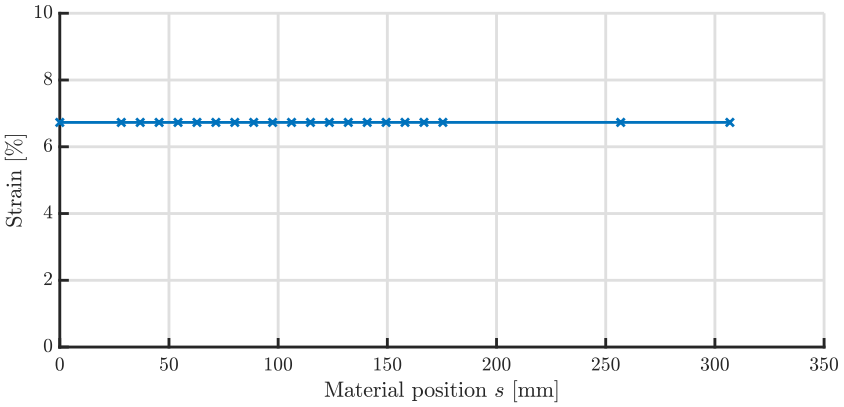

FIG. 12 – Evolution of the axial strain as a function of the material coordinate s.

from B to K. At first, a slip-only friction law of Coulomb type is considered as follows

$$T = \mu N \tag{81}$$

where N is the normal component of the reaction force of the cable on the pulley, which will be called the normal contact force and T is the tangential component of this reaction force, which will be called the friction force. μ is the kinetic friction coefficient. Considering that μ is known, the friction force to apply to every node on the pulley can be evaluated thanks to Eq. (81) if the normal contact force is known. In the present case, because nodes B to K are constrained to the pulley, the term $\mathbf{G}_{\text{spatial}}^T \boldsymbol{\lambda}_{\text{spatial}}$ in Eq. (74) represents the vector of reaction forces for each of these node. For node i, let us denote this force as $\mathbf{R}_i$. The normal component of the contact force N_i for each node i is found by projecting the reaction force $\mathbf{R}_i$ in the normal direction $\mathbf{n}_i$

$$N_i = \mathbf{R}_i \cdot \mathbf{n}_i \tag{82}$$

The friction force is then computed using Eq. (47) by replacing $\mathbf{t}_0$ with T computed through Eq. (81) and is applied to each node i in the tangential direction to the pulley. This friction force is thus computed as a pseudopunctual load acting on the material coordinates.

After running the simulation, the results can be validated by comparison with an analytical result. Indeed, according to the theory of belts and pulleys [6], the tension forces in the two branches of the (massless) cable are related through

$$\frac{F_1}{F_2} \leq e^{\mu \alpha_{\text{th}}} \tag{83}$$

where F_1 is the tension force in the tight branch, F_2 is the tension in the slack branch, and α_{th} is the theoretical angle of wrap of the cable on the pulley. The equality corresponds to the case where the slip limit is reached in the whole contact zone.

In order to reproduce this last case, a traction force is applied to the cable such that the displacement of the end node is nonzero but negligible. In this scenario, it can be considered that the slip threshold has just been reached, so that the ratio of tension forces should be exactly described by an exponential law. In the simulation, the traction force on node N is $F = 1000$ N, the Young's modulus of the cable is $E = 210$ GPa, its cross-sectional area is $A = 7.854$ mm^2, and the coefficient of friction is chosen as $\mu = 0.3$. There are $n = 20$ elements on the pulley from B to K. The length of the cable, the radius of the pulley and the regularization parameter are left unchanged compared to the previous simulation.

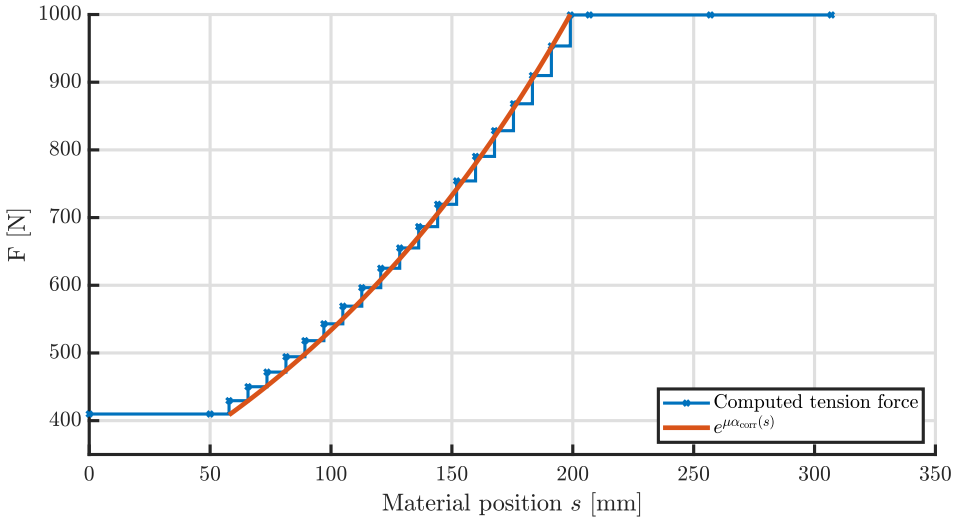

FIG. 13 – Evolution of the tension force in the cable for an angle of wrap $\alpha_{\text{corr}} = \pi - \dfrac{\pi}{20}$ rad and $\mu = 0.3$.

As nodes B and K are tangent to the pulley, no contact force develops between the cable and the pulley at these locations. This means that the friction force only departs from 0 for nodes $B+1$ to $K-1$. In the model, we thus consider that the first and last elements on the pulley are only in contact for half of their length. The angle of wrap considered in Eq. (83) is thus corrected as

$$\alpha_{\text{corr}} = \alpha_{\text{th}} - \frac{\alpha_{\text{th}}}{n} = \pi - \frac{\pi}{n} \tag{84}$$

where n is the number of elements on the pulley.

In Fig. 13, the evolution of the tension force in the cable is shown. It can be observed that it approaches the exponential law in Eq. (83) with $\alpha_{\text{corr}} = \pi - \pi/20$ rad in a staircase pattern, as the strain is constant in each element. Also, the global tension ratio F_1/F_2 exactly satisfies Eq. (83) with α_{corr}.

In the simulation, the number of elements $n = 20$ is finite, so that $\alpha_{\text{corr}} < \alpha_{\text{th}} = \pi$, leading to an underestimation of the tension ratio and thus to an overestimation of the tension force in the slack branch. However, the theoretical ratio should be reached for an infinite number of elements on the pulley as

$$\lim_{n\to\infty} \alpha_{\text{corr}} = \lim_{n\to\infty} \pi - \frac{\pi}{n} = \alpha_{\text{th}} \tag{85}$$

This property is illustrated in Fig. 14, where an order-1 convergence to the theoretical ratio $e^{\mu\pi}$ is observed when the number of elements on the pulley increases.

With 40 load steps, the average number of Newton iterations for the first regularized subproblem is 8.525. The second problem is not solved in this case because the cable motion is negligible at the slip limit.

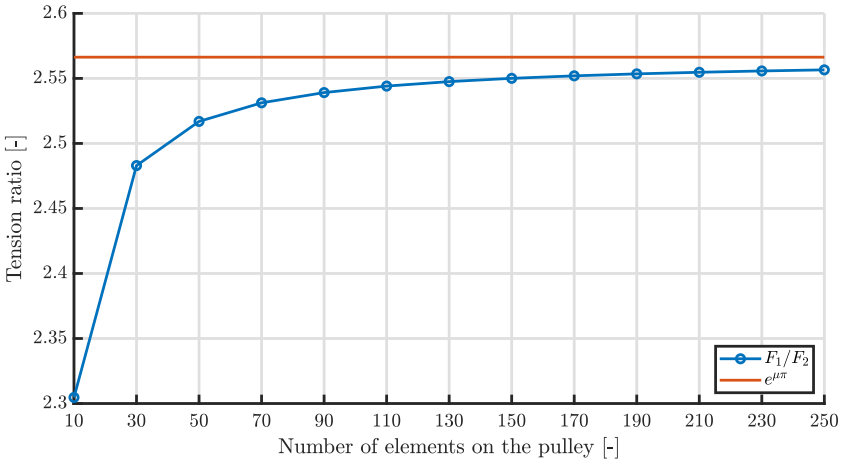

FIG. 14 – Evolution of the tension ratio as a function of the number of elements on the pulley.

4.4 Soft finger

Soft robots are robots made of soft materials, e.g., silicone or plastic. They exhibit various advantages. For instance, soft grippers grant flexibility to the tasks to be accomplished. Making use of adequate force and torque sensors, the same programming sequence can be used for the grasping of objects of different sizes and shapes, as can be encountered in the food industry [42, 43]. The actuation of soft robots may rely on different techniques, and cable-driven actuation is one of them. In the case of cable-actuated soft robots, the robot structure can either be entirely soft or composed of several relatively rigid sections connected together, as in the trunk considered in [4]. This is also notably the case for a soft finger composed of bulky phalanges with thin junctions, where a cable attached to the distal phalange can be used to control the bending of the finger, as shown in Fig. 15a. Even though the whole finger is made of soft material, deformations will mainly occur at the junctions between the phalanges due to the reduction in section. This kind of design has already been studied in the soft-robot community, for instance, a software toolkit for the modeling, simulation and control of soft robots is proposed in [5], a complete gripper made of three fingers is developed in [26], a self-healing material is used for the making of a finger in [38], and a soft finger actuated by three cables has been developed in [12]. The quasistatic simulation of a soft finger is thus studied in this section. The two phalanges are represented by rigid bodies, and their connection is modeled using a revolute joint with a torsional stiffness, simulating the local resistance of the junction to bending. The first phalange is fixed on a support. A punctual external force F is applied at the end of the cable while the other end is attached to the distal phalange. Although the proposed multibody model will not be able to catch the compliance of the phalanges, the main goal of the simulation is to show the interest of an ALE approach to model the interaction between the finger and the cable. Indeed, Fig. 15b illustrates the system under study and shows the position of the contact points between the phalanges and the cable inside its cavity. One observes that the positions of these points on the phalange are known *a priori* and that the rest of the cable is contact free, provided that the cable is under tension, so that the problem fits well to an ALE description.

Nodes are placed where contact and friction are supposed to happen. In Fig. 15c, these correspond to nodes B and C. Their spatial position is constrained to follow the motion of the finger and a flow of material can occur. Nodes A and D are also chosen to be constrained to

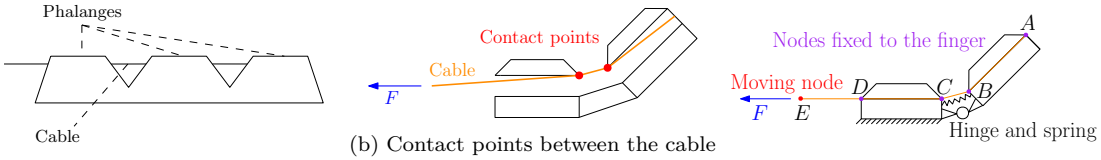

(a) Soft cable-actuated finger. (b) Contact points between the cable and the inside of the finger. (c) Numerical model of the finger.

FIG. 15 – Soft finger, occurrence of contact due to the cable actuation and associated numerical model.

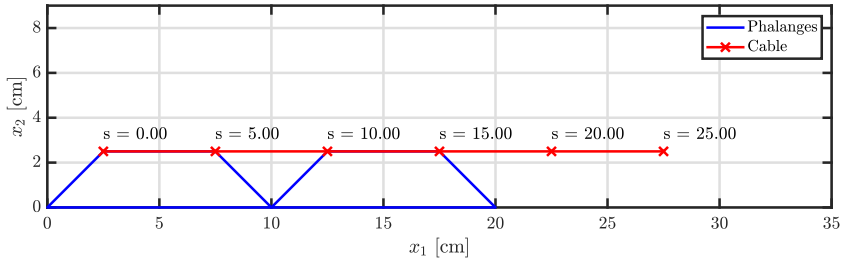

(a) Initial configuration.

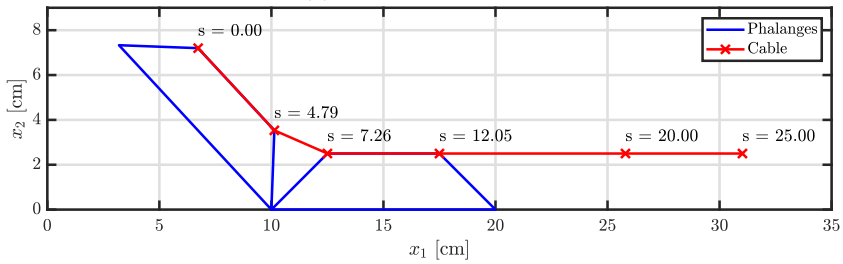

(b) Final configuration.

FIG. 16 – Soft-finger model actuated by a cable.

follow the motion of the phalanges. On the other hand, node E, and any node that would be located between nodes D and E can follow the material particles, as shown in Fig. 15c. The force $F = 1000$ N is applied in several load steps. The cable has an initial length $L = 25$ cm, a Young's modulus $E = 3$ GPa, and a cross-sectional area $A = 7.069$ mm^2. The torsional stiffness of the joint is equal to $k = 40$ N m. The regularization parameter α has been set to 1. The results are presented in Fig. 16. For the same reason as in Section 4.3.1, the node located between D and E at $s = 20$ cm keeps a fixed material position with the help of the regularization but any other material position between $s = 12.05$ cm and $s = 25$ cm for this node would be a valid solution to the problem. The flow of material is observed, as expected, at the contact points on the phalanges.

In terms of average number of Newton iterations, with 20 load steps, the first regularized subproblem converges in 4 iterations, whereas the second regularized subproblem converges in 1 iteration.

5 Discussion

This paper has presented a general ALE cable formulation with the following features.

1. It is possible to deal with nodes that are not considered Lagrangian or Eulerian *a priori*. In this case, the ALE solver establishes the solution to both the material and spatial equilibrium equations, such that the final mesh is optimal in an energetic sense. This property was illustrated in the clamped-clamped cable example by computing the energy for different material positions of the middle node in a Lagrangian setting.
2. When such material and spatial freedom is given at some nodes, the tangent stiffness matrix can become singular in several cases. First, as shown in the cable-pulley example, the set of equations may be redundant if the strain is uniform in adjacent elements and the solution is then not uniquely defined. Secondly, as shown in the clamped-clamped cable example, the tangent stiffness is locally singular at the undeformed configuration. A novel regularization procedure was proposed to build an algorithm converging to one of the solutions in all these cases.
3. Constraints can be taken into account to model driven motions or to represent interactions with other mechanical components of a multibody system. This capability was illustrated in the cable-pulley and in the cable-actuated soft-finger examples.

For the clamped-clamped cable example, the results are similar to those presented in [2] although a different material law is considered. In our formulation, the regularization was essential as the tangent stiffness matrix is singular at the undeformed configuration. In [2], this issue was not solved using a regularization but using a so-called dynamic constraint strategy. Our regularization is closer to the method proposed by [29] with the difference that our method is based on a sequence of two subproblems solved using a standard Newton scheme whereas the method in [29] was based on a single problem solved using a line-search scheme and a Cholesky factorization. Also, the formulation of constraints was not addressed in [2] nor in [29].

Several ALE cable formulations were developed in the multibody community and were combined with the description of constraints [8,18]. However, in these papers, the description of each node is *a priori* specified either as Lagrangian or Eulerian. As a consequence, the tangent stiffness matrix is not exposed to the aforementioned singularity issues and no regularization technique is needed. Our example includes an unconstrained node M that might undergo both material and spatial motions, thereby demonstrating the generality of our approach and the effectiveness of the proposed regularization, leading to an optimal mesh at convergence. In [17], a general dynamic framework is proposed with no *a priori* condition on the motion of the nodes. However, this paper does not address singularity issues, nor regularization techniques. It might be that the singularity issues are specific to quasistatic models.

Finally, the paper has shown that a cable-actuated soft finger can be modeled as a multibody system based on the proposed ALE formulation. This contrasts with usual approaches considered in the robotics community such as in [5], where a 3D mesh of the entire structure is used. A multibody model offers the advantage of a more concise model based on a limited number of nodes and coordinates in order to capture the interactions between the cable actuation and the finger motion.

6 Conclusion

In this paper, the arbitrary Lagrangian-Eulerian quasistatic formulation of a cable element in a multibody framework was revisited. Unlike many other ALE formulations in the multibody community, it starts from the continuous form of the equilibrium and uses the principle of virtual work before introducing the finite element discretization. This development may thus help to clarify the link between the continuum mechanics literature and the multibody dynamics literature for a simple cable. The resulting unidimensional cable finite element with a uniform

distribution of strains in the cross section was tested on elementary examples and was successfully used for the modeling of two multibody systems: a cable-pulley system and a cable-actuated soft finger.

As is known in the continuum mechanics literature and as illustrated in the clamped-clamped cable example, the configuration of the mesh resulting from the ALE simulation is energy optimal. This means that the mesh will find the material position yielding a global minimum of the potential energy in the cable. The advantage of such energy-optimal meshes is that they capture the displacement field better than a uniform mesh. Indeed, the reference displacement field obtained with a purely Lagrangian simulation and 800 elements is well approximated with only a few ALE elements.

The formulation is general and can be extended to the modeling of the interactions between cables and multibody systems. Constraints can be used to represent driven motions or connections between the components of the system. In the cable-pulley example, a frictionless simulation was performed for a cable subjected to an imposed displacement of both ends while keeping the nodes on the pulley spatially fixed thanks to constraints. It was shown that a flow of material occurs on the pulley, capturing the motion of the cable around the pulley. Then, a simple sliding friction model was considered. The normal contact force was retrieved from the Lagrange multiplier appearing in the equilibrium equations, which permits us to evaluate the tangential friction force according to Coulomb's law. The simulation was performed by imposing a traction force at the end of the cable so that the slip limit was reached. A comparison with the analytical result for the evolution of the tension force in the cable, which follows an exponential decrease, confirmed the validity of the proposed ALE formulation for cable-pulley systems.

Finally, the advantages of the formulation were also shown in the case of a cable-actuated soft finger, where contact and friction may also be considered between the cable and the finger cavity. This example demonstrated the possibility to directly couple the ALE cable formulation with normal multibody elements such as rigid bodies, representing the phalanges, and other constraints such as the revolute joint with a torsional stiffness located between the two phalanges. A frictionless model was considered in this paper. However, the same sliding friction model as for the pulley could be applied without further consideration.

In all those cases, a singularity of the tangent stiffness matrix, a nonconvexity of the problem and/or a nonuniqueness of the solution might arise. To overcome these issues, a regularization of the problem has been proposed by first solving a completely regularized subproblem, and then solving a partially regularized problem that only restrains the dependent material coordinates. In the considered examples, this second subproblem converges in less than two iterations on average, so that the computational overhead of the two-step procedure remains small and ensures the convergence of the solver to one of the possible solutions of the unregularized problem.

As perspectives, the present formulation could be adapted to more sophisticated elements, such as beam elements. This will permit study of other cases where the bending stiffness is non-negligible and to observe the mesh-optimality property under other types of loading. In a later step, the friction model should also be revisited. Although sliding friction was proposed in this paper for the cable-pulley example, this model can only be used under quite restrictive assumptions. A more general friction model could be explored to capture the stick-slip transition phenomenon and represent situations where the cable effectively drives the pulley. Finally, cables are often assumed to be unable to support compressive loads. The introduction of a noncompressibility condition might also be considered in a future generalization of the model.

Acknowledgements This work has been partly funded by the Robotix Academy project of the Greater Region. This project has also received funding from the European Union's Horizon 2020 research and innovation programme under the Marie Sklodowska-Curie grant agreement No 860124. The present paper only reflects the

authors' view. The European Commission and its Research Executive Agency (REA) are not responsible for any use that may be made of the information it contains.

Declarations

Ethical Approval

Not applicable

Funding

This work has been partly funded by the Robotix Academy project of the Greater Region. This project has also received funding from the European Union's Horizon 2020 research and innovation programme under the Marie Sklodowska-Curie grant agreement No 860124. The present paper only reflects the authors' view. The European Commission and its Research Executive Agency (REA) are not responsible for any use that may be made of the information it contains.

Competing interests

The authors declare that they have no competing interests.

Availability of data and materials

Not applicable

References

1. Arena, A., Pacitti, A., Lacarbonara, W.: Nonlinear response of elastic cables with flexural-torsional stiffness. International journal of solids and structures **87**, 267–277 (2016)
2. Askes, H., Kuhl, E., Steinmann, P.: An ALE formulation based on spatial and material settings of continuum mechanics. Part 2: Classification and applications. Computer methods in applied mechanics and engineering **193**(39-41), 4223–4245 (2004)
3. Bertrand, C.: Dynamics of a translating cable subjected to unilateral constraints, friction and punctual loads. Ph.D. thesis, Université de Lyon (2022)
4. Coevoet, E., Escande, A., Duriez, C.: Optimization-based inverse model of soft robots with contact handling. IEEE Robotics and Automation Letters **2**(3), 1413–1419 (2017)
5. Coevoet, E., Morales-Bieze, T., Largilliere, F., Zhang, Z., Thieffry, M., Sanz-Lopez, M., Carrez, B., Marchal, D., Goury, O., Dequidt, J., et al.: Software toolkit for modeling, simulation, and control of soft robots. Advanced Robotics **31**(22), 1208–1224 (2017)
6. Debongnie, J.F.: Conception et calcul des éléments de machine, dépôt légal d/2013/0480/7 edn. Debongnie Jean-François (May 2013)
7. Donea, J., Huerta, A.: Finite element methods for flow problems. John Wiley & Sons (2003)
8. Escalona, J.L.: An arbitrary Lagrangian–Eulerian discretization method for modeling and simulation of reeving systems in multibody dynamics. Mechanism and Machine Theory **112**, 1–21 (2017)
9. Escalona, J.L., Mohammadi, N.: Advances in the modeling and dynamic simulation of reeving systems using the arbitrary lagrangian–eulerian modal method. Nonlinear Dynamics **108**(4), 3985–4003 (2022)
10. Eshelby, J.: The elastic energy-momentum tensor. Journal of Elasticity **5**(3), 321–335 (1975)
11. Fu, K., Zhao, Z., Ren, G., Xiao, Y., Feng, T., Yang, J., Gasbarri, P.: From multiscale modeling to design of synchronization mechanisms in mesh antennas. Acta Astronautica **159**, 156–165 (2019)
12. Grube, M., Bekman, T., Seifried, R.: Modeling and advanced control for designing a soft material robot. In: 11th ECCOMAS Thematic Conference on Multibody Dynamics, Lisbon, Portugal

13. Grundl, K., Schindler, T., Ulbrich, H., Rixen, D.J.: ALE beam using reference dynamics. Multibody System Dynamics **46**(2), 127–146 (2019)
14. Guo, J., Huang, H., Yu, Y., Liang, Z., Ambrósio, J., Zhao, Z., Ren, G., Ao, Y.: Modeling muscle wrapping and mass flow using a mass-variable multibody formulation. Multibody System Dynamics **49**, 315–336 (2020)
15. Hagedorn, P., Schäfer, B.: On non-linear free vibrations of an elastic cable. International Journal of Non-Linear Mechanics **15**(4-5), 333–340 (1980)
16. Han, S.: Configurational forces and geometrically exact formulation of sliding beams in non-material domains. Computer Methods in Applied Mechanics and Engineering **395**, 115063 (2022)
17. Han, S., Bauchau, O.A.: Configurational forces in variable-length beams for flexible multibody dynamics. Multibody System Dynamics pp. 1–24 (2022)
18. Hong, D., Ren, G.: A modeling of sliding joint on one-dimensional flexible medium. Multibody System Dynamics **26**, 91–106 (2011)
19. Humer, A., Steinbrecher, I., Vu-Quoc, L.: General sliding-beam formulation: A non-material description for analysis of sliding structures and axially moving beams. Journal of Sound and Vibration **480**, 115341 (2020)
20. Irschik, H., Holl, H.: The equations of Lagrange written for a non-material volume. Acta Mechanica **153**(3), 231–248 (2002)
21. Irvine, H.M.: Cable structures. Constable Dover (1992)
22. Irvine, H.M., Caughey, T.K.: The linear theory of free vibrations of a suspended cable. Proceedings of the Royal Society of London. A. Mathematical and Physical Sciences **341**(1626), 299–315 (1974)
23. Kuhl, E., Askes, H., Steinmann, P.: An ALE formulation based on spatial and material settings of continuum mechanics. Part 1: Generic hyperelastic formulation. Computer Methods in Applied Mechanics and Engineering **193**(39-41), 4207–4222 (2004)
24. Kuhl, E., Hulshoff, S., De Borst, R.: An arbitrary Lagrangian Eulerian finite-element approach for fluid–structure interaction phenomena. International Journal for Numerical Methods in Engineering **57**(1), 117–142 (2003)
25. Lacarbonara, W., Pacitti, A.: Nonlinear modeling of cables with flexural stiffness. Mathematical Problems in Engineering **2008** (2008)
26. Manti, M., Hassan, T., Passetti, G., D'Elia, N., Laschi, C., Cianchetti, M.: A bioinspired soft robotic gripper for adaptable and effective grasping. Soft Robotics **2**(3), 107–116 (2015)
27. Maugin, G., Trimarco, C.: Pseudomomentum and material forces in nonlinear elasticity: Variational formulations and application to brittle fracture. Acta Mechanica **94**(1), 1–28 (1992)
28. Maugin, G.r.A.: Material forces: concepts and applications (1995)
29. Mosler, J., Ortiz, M.: On the numerical implementation of variational arbitrary Lagrangian–Eulerian (VALE) formulations. International Journal for Numerical Methods in Engineering **67**(9), 1272–1289 (2006)
30. Mueller, R., Maugin, G.: On material forces and finite element discretizations. Computational mechanics **29**(1), 52–60 (2002)
31. Oborin, E., Vetyukov, Y., Steinbrecher, I.: Eulerian description of non-stationary motion of an idealized belt-pulley system with dry friction. International Journal of Solids and Structures **147**, 40–51 (2018)
32. Pechstein, A., Gerstmayr, J.: A Lagrange–Eulerian formulation of an axially moving beam based on the absolute nodal coordinate formulation. Multibody System Dynamics **30**(3), 343–358 (2013)
33. Peng, Y., Wei, Y., Zhou, M.: Efficient modeling of cable-pulley system with friction based on arbitrary-Lagrangian-Eulerian approach. Applied Mathematics and Mechanics **38**(12), 1785–1802 (2017)
34. Pennisi, G., Bauchau, O.: Variational principles for non-material systems within an arbitrary Lagrangian Eulerian description of motion. In: International Design Engineering Technical Conferences and Computers and Information in Engineering Conference, vol. 83914, p. V002T02A018. American Society of Mechanical Engineers (2020)
35. Pieber, M., Ntarladima, K., Winkler, R., Gerstmayr, J.: A hybrid arbitrary lagrangian eulerian formulation for the investigation of the stability of pipes conveying fluid and axially moving beams. Journal of Computational and Nonlinear Dynamics **17**(5), 051006 (2022)
36. Rega, G.: Non-linearity, bifurcation and chaos in the finite dynamics of different cable models. Chaos, Solitons & Fractals **7**(10), 1507–1536 (1996)
37. Rega, G.: Nonlinear vibrations of suspended cables—part i: Modeling and analysis. Appl. Mech. Rev. **57**(6), 443–478 (2004)
38. Roels, E., Terryn, S., Brancart, J., Van Assche, G., Vanderborght, B.: A multi-material self-healing soft gripper. In: 2019 2nd IEEE International Conference on Soft Robotics (RoboSoft), pp. 316–321. IEEE (2019)
39. Rohrs, J.: On the oscillations of a suspended cable. Trans. Cambridge Philos. Soc **9**, 379–398 (1851)
40. Steinbrecher, I., Humer, A., Vu-Quoc, L.: On the numerical modeling of sliding beams: A comparison of different approaches. Journal of Sound and Vibration **408**, 270–290 (2017)
41. Vetyukov, Y.: Non-material finite element modelling of large vibrations of axially moving strings and beams. Journal of Sound and Vibration **414**, 299–317 (2018)
42. Wang, Z., Hirai, S.: A 3D printed soft gripper integrated with curvature sensor for studying soft grasping. In: 2016 IEEE/SICE International Symposium on System Integration (SII), pp. 629–633. IEEE (2016)

43. Wei, Y., Chen, Y., Ren, T., Chen, Q., Yan, C., Yang, Y., Li, Y.: A novel, variable stiffness robotic gripper based on integrated soft actuating and particle jamming. Soft Robotics **3**(3), 134–143 (2016)
44. Wu, Q., Takahashi, K., Nakamura, S.: Formulae for frequencies and modes of in-plane vibrations of small-sag inclined cables. Journal of Sound Vibration **279**(3-5), 1155–1169 (2005)
45. Zielonka, M., Ortiz, M., Marsden, J.: Variational r-adaption in elastodynamics. International journal for numerical methods in engineering **74**(7), 1162–1197 (2008)